NASA Technical Paper 1130

Statistical Model for Asperity-Contact Time Fraction in Elastohydrodynamic Lubrication

Steven M. Sidik
Lewis Research Center
Cleveland, Ohio
and
John J. Coy
Propulsion Laboratory
U.S. Army R&T Laboratories (AVRADCOM)
Cleveland, Ohio

NASA

NASA Technical Paper 1130

Statistical Model for Asperity-Contact Time Fraction in Elastohydrodynamic Lubrication

Steven M. Sidik and John J. Coy

FEBRUARY 1978

National Aeronautics
and Space Administration

**Scientific and Technical
Information Office**

1978

STATISTICAL MODEL FOR ASPERITY-CONTACT TIME FRACTION IN ELASTOHYDRODYNAMIC LUBRICATION

by Steven M. Sidik and John J. Coy*

Lewis Research Center

SUMMARY

The theory of two-dimensional Gaussian random processes was applied to determine the time fraction during which there is asperity contact as a function of nominal elastohydrodynamic (EHD) film thickness. Calculations were based on profile traces obtained from typical bearing surfaces. The profile records were converted to digital form for statistical analysis. Moments to fourth order of the power spectral density function were computed and in turn used to calculate the probability distribution of local film thickness minima where asperity contact is likely to occur. Finally, the asperity-contact time fraction was calculated as a function of dimensionless film thickness ratio Λ by using two different methods. The number of asperity contacts per unit area of the nominal contact was also determined.

The results were applied to obtain numerical results for a 20-millimeter-bore ball bearing with three 7.15-millimeter (9/32-in.) balls. The contact time fraction was calculated for axial thrust loads of 90, 445, and 3100 newtons (20, 100, and 700 lb). The contact time fraction varied from almost no contact to almost full contact (1 percent to 90 percent) in a relatively narrow range of Λ (4 to 5). Full contact occurred at a film thickness ratio several times larger than that commonly reported in the literature where one-dimensional random process models were used.

INTRODUCTION

Elastohydrodynamic lubrication (EHD) is the term used to describe part of the technology concerning lubrication of concentrated mechanical contacts. EHD technology is particularly important and useful in the design and analysis of rolling-element bearings and gears.

*Propulsion Laboratory, U.S. Army R&T Laboratories (AVRADCOM).

Concentrated mechanical contacts are often called Hertzian contacts in honor of Heinrich Hertz, who first published a theory on the contact of elastic solids (ref. 1). In general, Hertzian contacts are flat and bounded by an ellipse that is small when compared with the radius of curvature at the point of contact. The Hertzian-contact pressure distribution is parabolic over the contact ellipse. For lubricated bodies in rolling contact a more comprehensive analysis is given by EHD theory. Both the shape of the contact zone and the pressure distribution are different from those given by Hertz's theory. References 2 to 5 are of general interest. In essence, EHD lubricant film formation depends on the coupled effects of physical changes in the lubricant, which are caused by high pressures in the Hertzian contact area, and elastic changes in the shape of the Hertzian contact area, which affect the pressure distribution. The high pressures in the EHD contact area act to squeeze out the lubricant. However, the lubricant becomes thicker (more viscous) with increasing pressure and resists being squeezed out. The net result is the formation of a thin lubricant film that is beneficial in preventing seizure and rapid wear of the contacting parts. Knowledge of the EHD film thickness is also essential for accurate prediction of fatigue life (ref. 6).

In evaluating the effect of various parameters on EHD film formation, physical experimentation is necessary. For many applications the EHD film thickness is the same order of magnitude as the surface rms roughness. Experimental measurement of the film thickness is very difficult because films are so thin. Various methods that have been used are optical (interferometry), X-ray, and electrical capacitance and conductance techniques (ref. 7). Of the aforementioned measurement methods, the capacitance and conductance methods are most suited to measurement of film thickness in full-scale bearings. The conductance method of measurement depends on having a known relation between film thickness and contact time fraction. The contact time fraction is directly related to the normalized average voltage observed when a low voltage is applied across the lubricant film.

In 1964, Tallian and his coworkers (ref. 8) formulated a statistical model of bearing surface roughness and used the model to infer EHD film thicknesses, based on electrical conductance measurements. Their results were applicable to the regime of "partial EHD contact," where the load is shared by the EHD film and the high points or asperities of the metal surfaces that momentarily interrupt the lubricant film (ref. 9).

By the early 1970's it was generally accepted that partial EHD contact must be viewed as a random process (refs. 9 to 12). Most researchers used stylus traces of the surface to obtain profile statistics for the random process models. In 1971, Nayak (ref. 13) explained how Longuet-Higgins' theory of ocean surfaces (refs. 14 to 16) could be used to model rough surfaces as two-dimensional, isotropic, Gaussian random processes. He showed that significant differences exist between surface statistics and profile statistics and that a naive analysis assuming that profile statistics may be

directly used is erroneous (refs. 13 and 17). Sidik has extended the theory of Nayak to obtain a model for asperity-contact time fraction as a function of film thickness in partial EHD contact lubrication (ref. 18). In reference 19, the theory is generalized to nonisotropic Gaussian surfaces.

The objective of the work described in this report was to apply the relevant results of two-dimensional random surface analysis to obtain a relation between asperity-contact time fraction and average EHD film thickness for a typical ball bearing that is used in the NASA EHD test rig.

THEORY RELATING CONTACT TIME FRACTION TO FILM THICKNESS

The ball bearing for which this analysis was performed has a 20-millimeter bore and three 7.15-millimeter- (9/32-in.-) diameter balls, figure 1. The contact angle is 17°, and the inner and outer race conformities are 53 and 54 percent, respectively. The pitch diameter is 35.5 millimeters (1.4 in.). Three different thrust loads were considered in the analysis of contact time fraction. Table I gives the calculated Hertzian stresses and contact ellipse dimensions corresponding to the different loads.

Bearing surfaces are herein represented as two-dimensional Gaussian random processes. The mathematical techniques are defined in appendix A. Longuet-Higgins (refs. 14 to 16) and Nayak (refs. 13 and 17) have examined the geometrical properties of random surfaces. In particular, they have derived expressions for the distributions of heights of summits, mean curvatures of summits, slopes of profiles, and expected density of maxima. In a recent paper, Adler and Hasofer (ref. 20) have defined an "upcrossing" of a random surface above a particular level and derived an expression for the expected number of such upcrossings per unit area of the reference plane. Relevant results from this reference are used in the results and discussion section of this report. Pertinent geometrical considerations from the aforementioned references are presented in appendix B.

Under loaded conditions, assume that the ball and race surfaces are two-dimensional ergodic Gaussian processes and that within the Hertzian contact zone the mean planes are parallel and separated by a lubricant film of thickness h. A cross section of a single ball-race contact is presented in figure 2. Coordinate x is in the direction of rolling. The ball surface is denoted by $z_b(x, y)$ and the race surface by $z_r(x, y)$. The two processes z_b and z_r are independent, with mean levels $\mu_b = 0$ and $\mu_r = 0$, correlation functions R_b and R_r, and variances σ_b^2 and σ_r^2, respectively.

The composite process $z = z_b + z_r$ is also an ergodic Gaussian process with mean zero and correlation function R and variance σ^2, where

$$\sigma^2 R(\tau_x, \tau_y) = \sigma_b^2 R_b(\tau_x, \tau_y) + \sigma_r^2 R_r(\tau_x, \tau_y) \tag{1}$$

With this notation, then (as shown in fig. 3) any metallic contact occurrence is represented by the composite surface rising above the level h.

An approximation to the time fraction during which there is metallic contact anywhere within the Hertzian zone will now be derived. This derivation is motivated by the problem described by Tallian (ref. 8), where this relation was used to measure EHD film thickness.

Consider the process z above the x-y plane. At a level h above the reference plane, pass a cutting plane that will occasionally intersect z. The sets of points in the reference plane where $z(x, y) \geq h$ are called excursion sets. Such excursion sets are represented as the crossed areas in figure 4. Superimposed upon this plane is an elliptical region that represents the Hertzian contact area. For constant rolling velocity, this elliptical region moves to the right at a constant velocity v through the region bounded by the parallel dashed lines y_1 and y_2. At the termination of a test period of time T the Hertzian area is at the elliptical region at the right in figure 4.

If it is assumed that $\Lambda = h/\sigma$ is large, the number of excursion sets is reasonably represented by a Poisson process. In this event, there will be few excursions of z above h and, hence, few metallic contacts. The contacts will be small in area, and the probability of two or more contacts in a small area is negligible. The contact occurrence is as follows: The dashed ellipse on the left in figure 4 represents the location of the Hertzian area when the contact is first made. The dashed ellipse on the right represents the location of the Hertzian area when the contact is broken. The two points $P(x_M, y_M)$ and $P(x_B, y_B)$ denote coordinates of the make-contact and break-contact occurrences. The distance of $P(x_B, y_B)$ to the centerline of the ellipse on the right is termed L_B. Thus, contact exists for a total distance L that is composed of three parts. Two of these parts are L_M and L_B; the third is termed X and is the distance $x_M - x_B$. From the Poisson assumptions, X is negligible with respect to L_M and L_B and the excursions are uniformly distributed with respect to the y-axis. Also L_M and L_B are approximately equal. As a result,

$$E\{L\} \cong 2E\{L_M\} = \frac{\pi l}{2} \tag{2}$$

where $\pi l/2$ is the average length of the Hertzian ellipse. The expected total contact time $E\{T^*\}$ can be approximated by the product of the average number of excursions and the average time of contact for each. Equivalently, $E\{T^*\}$ can be approximated by the average number of excursions per unit area $E\{\chi\}$ times the area rolled over, times the average time of contact for each. If T is large, the rolled-over area is

approximately vTw, so that

$$E\{T^*\} = E\{\chi\}(vTw)\left(\frac{\pi l}{2v}\right) \tag{3}$$

The expected contact time fraction is obtained as

$$E\{T_c\} = \frac{E\{T^*\}}{T} = \frac{\pi l w}{2} E\{\chi\} \tag{4}$$

Thus, $E\{T_c\}$ as a function of Λ can be calculated directly from a computation of $E\{\chi\}$ as a function of Λ. The derivation of $E\{\chi\}$ is presented in appendix B, where it is shown how $E\{\chi\}$ is computed from the lower order moments of the power spectral density function of the composite surface process.

The derivation to this point provides contact time fraction as a function of h for a single Hertzian contact. Next, the results are applied to a ball bearing with three balls for three different loads. It is assumed that at each of the six ball-race contacts the mean film thickness is the same and that each contact is statistically independent of the others. Because of the geometry of the balls and the race, however, the nominal Hertzian areas at the inner and outer race contacts are different. Table I presents the calculated conditions at these contacts for three different loads. From equation (4) it is evident that $E\{T_c\}$ is simply the area of the Hertzian contact times $E\{\chi\}$.

Let $T_{c,in}$ and $T_{c,out}$ denote the expected contact time fractions at the inner and outer races for a single ball. Thus, the probability of no contact on a single ball is $1 - T_{c,in}T_{c,out}$. From the independence assumption, the probability of no contact on any of the three balls is the quantity

$$1 - T_{c,ov} = (1 - T_{c,in}T_{c,out})^3 \tag{5}$$

and the expected overall contact fraction is thus

$$T_{c,ov} = 1 - (1 - T_{c,in}T_{c,out})^3 \tag{6}$$

Surface Measurement and Analysis

The first step in determining the expected number of excursions per unit area is to obtain and analyze surface profile traces from the bearing surfaces. By using these profile traces, the important surface parameters are computed as outlined in the pre-

vious section. Samples of the microtopography of bearing surfaces were obtained by using a surface finish inspection machine. The stylus used to obtain the traces had a tip radius of 0.00025 centimeter (0.0001 in.). The traces were recorded on the standard paper from the inspection machine and also recorded as a frequency-modulated (FM) signal on magnetic tape for digitizing and further analysis. As explained in appendix A, in order to characterize the surface statistics, one must first obtain profile traces in at least three different directions. The surfaces of the ball and race specimens were sampled to obtain records of the surface profile. Several traces in different directions on the ball surface showed that it was an isotropic surface. However, the race surface was not isotropic. In addition, it was very difficult to obtain a sample record on the race surface in any direction other than the rolling direction and the ball radius direction.

In order to obtain the necessary additional traces, a flat specimen was prepared by material and finishing methods identical to those used in making the bearing race. The flat specimen was approximately 2.5 by 5.0 centimeters (1 by 2 in.) with a 0.13- to 0.25-micrometer (5- to 10-μin.) CLA surface finish. Similarly, a surrogate ball, 14.3 millimeters (9/16 in.) in diameter with a 0.03- to 0.05-micrometer (1- to 2-μin.) CLA surface finish, was used to obtain sample ball records of sufficient length.

Figures 5 and 6 show the microtopography of the ball and the flat specimen. The traces shown in the figure were generated by making repeated traces in parallel directions. The trace lines are spaced on the graph approximately to the same scale as in the trace direction. For the ball in figure 5(b) the traces are 6.4 micrometers (0.00025 in.) apart, which is the limit of the tracing machine's resolution for sideways adjustment. For the flat specimen in figure 6(b) the traces are 63.5 micrometers (0.0025 in.) apart. In general, the adjacent traces are highly uncorrelated for the ball, which is expected from the method of manufacture. The flat specimens show evidence of grinding marks or grooves that run for 500 to 750 micrometers (0.020 to 0.030 in.).

Traces to be analyzed were recorded for three different directions on the ball and six different directions on the flat specimen. Nominally, the traces were taken 45° apart for the ball and 18° apart for the flat specimen. The first trace on the flat specimen was taken in the direction of the lay of the surface finish. This is the rolling direction for the ball in the race. Five more traces were taken, with the last trace being at 90° to the lay of the surface finish. The traces were taken several times and were found to be exactly repeatable.

As mentioned previously, the raw surface data were recorded in analog form as an FM signal on magnetic tape. This tape was sampled at equal intervals and written in digital format on another tape. The sampling intervals and the number of sampled points, along with the total sampled length, are presented in table II.

Each of the digitized profile traces was processed by a computer program that performed the following seven steps:

(1) Plotted the input data

(2) Performed a moving-average trend removal

(3) Plotted the centered and detrended data

(4) Plotted a frequency polygon of the relative surface heights

(5) Provided a normal probability plot of the sample cumulative distribution function

(6) Estimated the zeroth-, second-, and fourth-order moments by a differencing method for that profile

(7) Estimated the correlation function for that profile to five lag spacings and computed the second and fourth derivatives of the correlation function by using finite difference approximations

The results are given in the following section.

Profile Analysis

Plotted input. - All the plots were examined for faithful reproduction of the original record and were visually found to be identical. For the sake of brevity, only the first 0.1 centimeter of trace 10 is shown as a typical result in figure 7.

Moving-average trend removal. - The raw data required detrending for two reasons. First, the stylus head does not follow a path parallel to the mean line of the profile when tracing. This causes a linear trend. The other reason for detrending was to anticipate the detrending that occurs naturally in the lubrication process. Therefore, it was decided to remove trends with wavelengths longer than the Hertzian contact. The moving-average trend remover, which is essentially a high-pass filter, was effective in removing these trends.

The trend removal consisted of taking the input data record represented as $z_1, \ldots, z_N$ and replacing it by a new record $Z_1, \ldots, Z_{N-K}$, where

$$Z_{i-\frac{K}{2}} = z_i - \bar{z}_i \tag{7}$$

where

$$\bar{z}_i = \frac{1}{K+1} \sum_{j=i-\frac{K}{2}}^{i+\frac{K}{2}} z_j$$

and K must be even. The number of points in the moving average is a function of the sample interval and the load since the contact ellipse dimensions change with load. The number of points for each load and each profile are given in table III.

Plotted centered and detrended data. - The first 0.1 centimeter of trace 10, after centering and moving-average removal, is given in figure 8.

Frequency polygons. - A frequency polygon or histogram was constructed and plotted for each detrended profile by determining the maximum and minimum surface heights attained and dividing into k equal intervals (up to k = 100).

$$k = 1 + 4(\log N)^2 \tag{8}$$

The data record was then scanned, and the frequency f_i of heights in each interval was recorded. A sample frequency polygon for trace 10 is presented in figure 9. The frequency polygons indicated a general agreement with Gaussian distributions.

Normal probability plot. - A simple graphical test for normality is to plot the sample cumulative distribution function on Gaussian probability paper. The ordinate is the proportion of observations in the sample that are less than or equal to h. The abscissa is the relative height. If a plotted sample were to exactly represent a normal distribution, the resulting points would fall on a straight line.

Plots for all sample records are provided in figure 10.

Estimated spectral moments. - There are several methods that might be used to estimate the spectral moments of the surface profile process. Lindgren (ref. 21) discusses several, but a detailed comparison of the methods is not yet available. The method chosen here is as follows: The spectral moments are given by the variance of derivatives

$$\left.\begin{aligned} m_0 &= \mathrm{VAR}\left[Z(t_i)\right] \\ m_2 &= \mathrm{VAR}\left[Z'(t_i)\right] \\ m_4 &= \mathrm{VAR}\left[Z''(t_i)\right] \end{aligned}\right\} \tag{9}$$

where the derivatives are approximated by differences

$$\left.\begin{aligned} Z'(t_i) &= \frac{Z(t_i) - Z(t_{i-1})}{\Delta} \\ Z''(t_i) &= \frac{Z'(t_i) - Z'(t_{i-1})}{\Delta} \\ \Delta &= t_i - t_{i-1} \end{aligned}\right\} \tag{10}$$

and VAR( ) is the sample variance operator. Table IV presents the estimated moments for the three load conditions.

The rms roughness of the surface is estimated by $m_0^{1/2}$. Note that m_0 is approximately the same for each ball trace. For the flat surface, m_0 decreases almost monotonically as the angle increases to 90^o. Theoretically, m_0 should be independent of direction. We do not have an explanation for m_0 varying with direction.

The values of m_2 for the ball traces are quite close for traces 2 and 3 but somewhat smaller for trace 1. Theoretically, they should all be the same. There is no obvious reason for trace 1 and traces 2 and 3 to be different.

The values of m_2 for the flat traces increase monotonically from the 0^o to the 90^o angle traces. This is to be expected since traces 4 to 9 are sequentially taken from the direction of lay to directly across the lay.

The values of m_4 for the ball traces are quite close for traces 2 and 3 but somewhat smaller for trace 1. Theoretically, they should all be the same. There is no obvious reason for trace 1 and traces 2 and 3 to be different. The values of m_4 are all roughly the same for each of the flat traces.

Estimated correlation functions. - The correlation function for each profile was estimated by the definitional formula

$$R_k = \frac{\sum_{i=1}^{N-k} (Z_i - \overline{Z})(Z_{i+k} - \overline{Z})}{\sum_{i=1}^{N} (Z_i - \overline{Z})^2} \tag{11}$$

for $k = 1,5$. This was done because there is a well-known relation between spectral moments and derivatives of R evaluated at the origin (ref. 22),

$$m_{2i} = m_0(-1)^i R^{(2i)}(0) \tag{12}$$

This relation serves as a way to check the general accuracy of the moment estimations described in the previous section. The derivatives are calculated by the difference approximations:

$$
\left.
\begin{aligned}
R_3^{(2)} &= -\frac{2(R_0 - R_1)}{\Delta^2} \\
R_5^{(2)} &= -\frac{15R_0 - 16R_1 + R_2}{6\Delta^2} \\
R_7^{(2)} &= -\frac{245R_0 - 270R_1 + 27R_2 - 2R_3}{90\Delta^2} \\
R_5^{(4)} &= \frac{2(3R_0 - 4R_1 + R_2)}{\Delta^4} \\
R_7^{(4)} &= \frac{28R_0 - 39R_1 + 12R_2 - R_3}{3\Delta^4}
\end{aligned}
\right\} \tag{13}
$$

where $R_j^{(i)}$ denotes the i^{th} derivative approximated by a j point symmetric finite difference (ref. 23). The correlation functions for the 90-newton (20-lbf) load-case and the resulting moment estimates are given in table V and plotted in figures 11 and 12. The moments obtained are approximately the same as those obtained by using equations (9) and (10) (table IV).

COMPOSITE SURFACE ANALYSES

Up to this point, each trace has been analyzed as a separate profile from the appropriate surface. It is now time to pool the information from these profiles to obtain a description of the surfaces in their two-dimensional forms. This is achieved by mathematically combining the surfaces to obtain the statistics for the composite process. The process consists of three stages, averaging the ball moments, adding ball moments to flat profile moments, and estimating spectral moments by least squares. The stages are discussed separately.

Averaging ball moments. - Ball surfaces are typically finished in such a manner that there is no preferential direction for surface lay. This is described statistically by calling the surface isotropic. For the ball surface the three separate profiles can

be considered to provide three independent observations. Therefore, the average moments for the ball are given by

$$\left.\begin{aligned} m_0^b &= \frac{1}{3}\sum m_{0i} \\ m_2^b &= \frac{1}{3}\sum m_{2i} \\ m_4^b &= \frac{1}{3}\sum m_{4i} \end{aligned}\right\} \tag{14}$$

Adding ball moments to flat profile moments. - According to the definitional equation for spectral moments (eq. (A8)), the spectral moments of a profile of the composite surface are simply the sums of the appropriate individual surface moments. The n^{th} moment of a composite profile in direction θ is denoted by $m_{n,\theta}$, the n^{th} moment of the flat surface in direction θ by $m^f_{n,\theta}$, and the n^{th} moment of the ball profile by m^b_n. Hence, it is true that

$$m_{n,\theta} = m^b_n + m^f_{n,\theta} \tag{15}$$

Table IV shows that the moments of the flat surface dominate the ball surface for all loads.

Estimating spectral moments by least squares. - The following relations between the two-dimensional moments m_{ij} and the profile moments $m_{n,\theta}$ were obtained from equation (A9).

$$m_{0,\theta} = m_{00} = \sigma^2_\theta \tag{16}$$

$$m_{2,\theta} = m_{20}\cos^2\theta + 2m_{11}\cos\theta\sin\theta + m_{02}\sin^2\theta \tag{17}$$

$$m_{4,\theta} = m_{40}\cos^4\theta + 4m_{31}\cos^3\theta\sin\theta + 6m_{22}\cos^2\theta\sin^2\theta + 4m_{13}\cos\theta\sin^3\theta + m_{04}\sin^4\theta \tag{18}$$

Equation (16) implies that the best estimator for m_{00} is simply the average of the $m_{0,\theta}$. The results for m_{00} are 5.97×10^{-2}, 6.41×10^{-2}, and 5.90×10^{-2} square micrometer, respectively, for loads of 90, 445, and 3100 newtons (20, 100, and 700 lbf).

Equation (17) provides one equation for each θ, or a total of seven equations in

three unknowns. For each load the estimates for m_{20}, m_{11}, and m_{02} are given here in a matrix format, emphasizing that this represents the covariance matrix of φ_x and φ_y in the spectral density function. The matrices are nearly diagonal, which means that the distributions of φ_x and φ_y are effectively uncorrelated. For the 90-newton (20-lbf) load,

$$\begin{bmatrix} m_{20} & m_{11} \\ m_{11} & m_{02} \end{bmatrix} = \begin{bmatrix} 2.39\times10^{-3} & 3.4\times10^{-5} \\ 3.4\times10^{-5} & 5.73\times10^{-3} \end{bmatrix} \tag{19}$$

For the 445-newton (100-lbf) load,

$$\begin{bmatrix} m_{20} & m_{11} \\ m_{11} & m_{02} \end{bmatrix} = \begin{bmatrix} 2.22\times10^{-3} & 1.31\times10^{-4} \\ 1.31\times10^{-4} & 5.58\times10^{-3} \end{bmatrix} \tag{20}$$

For the 3100-newton (700-lbf) load,

$$\begin{bmatrix} m_{20} & m_{11} \\ m_{11} & m_{02} \end{bmatrix} = \begin{bmatrix} 2.17\times10^{-3} & -4.4\times10^{-5} \\ -4.4\times10^{-5} & 5.66\times10^{-3} \end{bmatrix} \tag{21}$$

Equation (18) provides one equation for each θ, hence, seven equations in the five unknowns m_{40}, m_{31}, m_{22}, m_{13}, and m_{04}. For each load the estimates of these moments are as follows: For the 90-newton (20-lbf) load,

$$\begin{bmatrix} m_{40} & m_{31} & m_{22} \\ m_{31} & m_{22} & m_{13} \\ m_{22} & m_{13} & m_{04} \end{bmatrix} = \begin{bmatrix} 6.65\times10^{-2} & 3.88\times10^{-4} & 1.89\times10^{-2} \\ 3.88\times10^{-4} & 1.89\times10^{-2} & 2.14\times10^{-3} \\ 1.89\times10^{-2} & 2.14\times10^{-3} & 7.27\times10^{-2} \end{bmatrix} \mu m^{-2} \tag{22}$$

For the 445-newton (100-lbf) load,

$$\begin{bmatrix} m_{40} & m_{31} & m_{22} \\ m_{31} & m_{22} & m_{13} \\ m_{22} & m_{13} & m_{04} \end{bmatrix} = \begin{bmatrix} 6.61\times10^{-2} & 3.13\times10^{3} & 1.55\times10^{-2} \\ 3.13\times10^{3} & 1.55\times10^{-2} & 4.39\times10^{-3} \\ 1.55\times10^{-2} & 4.39\times10^{-3} & 7.20\times10^{-2} \end{bmatrix} \mu m^{-2} \tag{23}$$

For the 3100-newton (700-lbf) load,

$$\begin{bmatrix} m_{40} & m_{31} & m_{22} \\ m_{31} & m_{22} & m_{13} \\ m_{22} & m_{13} & m_{04} \end{bmatrix} = \begin{bmatrix} 6.49\times10^{-2} & 4.50\times10^{-3} & 1.51\times10^{-2} \\ 4.50\times10^{-3} & 1.51\times10^{-2} & 5.33\times10^{-3} \\ 1.51\times10^{-2} & 5.33\times10^{-3} & 7.05\times10^{-2} \end{bmatrix} \mu m^{-2} \tag{24}$$

From appendix A, equation (A10), a spectrum or random process is isotropic if

$$\left.\begin{aligned} m_{11} = m_{13} = m_{31} = 0 \\ m_{20} = m_{02} = m_2 \\ m_{40} = m_{04} = 3m_{22} = m_4 \end{aligned}\right\} \tag{25}$$

Note that m_{11}, m_{13}, and m_{31} are much smaller than the other moments. Also, m_{04} and m_{40} are approximately equal to each other and to $3m_{22}$. The fourth-order moments thus satisfy isotropy conditions. Further examination, however, shows that m_{02} is approximately twice m_{20}. The second-order moments thus satisfy an elliptical isotropy condition. A process is elliptically isotropic if

$$R(\tau_x, \tau_y) \approx R(l)$$

where

$$l^2 = a\tau_x^2 + \tau_y^2 \tag{26}$$

for some $a > 0$. Webber (ref. 24) discusses methods of treating such processes.

RESULTS AND DISCUSSION

The final result of this analysis was obtained by using the moment estimates for the two-dimensional process to calculate the expected number of crossings per unit area (eqs. (B8) to (B12)) for various film thickness ratios. These expectations were then used to obtain the contact time fraction T_c (eqs. (4) to (6)). The results are presented in table VI. Curves of contact time fraction against film thickness ratio are plotted in figure 13. The calculations for these results required some 30 hours of computer time.

For comparison, values of $E\{\chi\}$ were calculated from the spectral moments by using the method of Adler and Hasofer (eq. (B13)). Table VII presents the values of $E\{\chi\}$ and the resulting contact time fractions. Figure 14 gives the contact time fraction curves from the method of Adler and Hasofer, which may be compared to the NASA results in figure 13. Both sets of curves are similar in shape and in the spacing between the different loads. The NASA curves are shifted toward higher values of Λ by an amount approximately equal to 0.35. The reason for this difference is unclear. Both methods should be asymptotically equivalent, and values of Λ greater than 4 should be sufficiently large for the asymptotic results to hold. Adler and Hasofer's "upcrossings" seem closer to the required "excursion sets" in the development of contact time fraction than the approximation based on peak height distribution. Nevertheless both are approximations. At this point it is not known which is the best.

Some comments are needed regarding the usefulness of these curves as a means of measuring film thickness by the electrical conductance method of Tallian (ref. 8). Previous work has indicated that the contact time fraction begins to increase from zero at $\Lambda \approx 3$ and monotonically increases until there is 100-percent contact at $\Lambda \approx 1$. By comparison the results of this investigation show this same change in contact time fraction occurring for film thicknesses several times larger. Also, the incremental change in film thickness corresponding to the incremental change from no contact to 100-percent contact is smaller. Therefore, the usefulness of the model is limited to a narrow range of film thickness for any given constant load. The theoretical differences in probability distributions for peak heights of summits on a two-dimensional surface and peak heights on profile traces along a fixed direction on the surface may account for these differences.

SUMMARY OF RESULTS

Relations for asperity-contact time fraction as a function of nominal elastohydrodynamic (EHD) film thickness have been presented. The calculations were based on a two-dimensional random surface model. Results were obtained for a 20-millimeter-bore ball bearing with three 7.15-millimeter (9/32-in.) balls. Surface traces were obtained by using a profilometer, and a statistical analysis was performed in which the profile traces were used as statistical sample records. Histograms, spectral moments, and the number of asperities per unit area were obtained. The investigation yielded the following results:

1. The contact time fraction varied from almost full contact (90 percent) to almost no contact (1 percent) in the dimensionless film thickness range 4 to 5. Full contact occurred at a film thickness ratio several times larger than commonly reported in the literature.

2. The composite surface process is approximately elliptically isotropic.

3. The surfaces measured were only approximately Gaussian.

4. The usefulness of the curves of contact time fraction as a means of determining film thickness by electrical conductance measurements is limited to a narrow range of film thickness ratio.

Lewis Research Center,
National Aeronautics and Space Administration,
Cleveland, Ohio, September 13, 1977,
505-04.

APPENDIX A

CORRELATION AND POWER SPECTRAL DENSITY FUNCTIONS

The probabilistic behavior of an ergodic Gaussian random surface is entirely defined by either the correlation function R or the power spectral density (psd) function $\mathscr{S}$. They are Fourier transform pairs. A Gaussian random process $z(x, y)$ is one (1) that follows a Gaussian distribution with mean μ and variance σ^2 and (2) for which, for all finite n and values of $\tau_{x,i}$ and $\tau_{y,i}$ $(i = 1, n)$, the variables $z(x + \tau_{x,i}, y + \tau_{y,i})$ follow joint multivariate normal distributions. In this report the correlation function is defined as

$$R(\tau_x, \tau_y) = \frac{1}{\sigma^2} E\left\{\left[z(x + \tau_x, y + \tau_y) - \mu\right]\left[z(x, y) - \mu\right]\right\} \tag{A1}$$

This function measures the degree of relation between the heights of the random surface above two points of the reference plane that are a fixed distance and direction apart.

The ergodic assumption states that the statistics of the process are not a function of x and y. Therefore, the expectation may be taken in the ensemble sense as in equation (A1) or as an average over the x-y plane as follows:

$$R(\tau_x, \tau_y) = \lim_{\substack{T_x \to \infty \\ T_y \to \infty}} \frac{1}{\sigma^2} \frac{1}{2T_x} \frac{1}{2T_y} \int_{-T_x}^{T_x} \int_{-T_y}^{T_y} \left[z(x + \tau_x, y + \tau_y) - \mu\right]\left[z(x, y) - \mu\right] dy\, dx \tag{A2}$$

The psd is the Fourier transform of R given by

$$\mathscr{S}(\varphi_x, \varphi_y) = \frac{1}{(2\pi)^2} \int_{-\infty}^{\infty} \int_{-\infty}^{\infty} \exp\left[-i(\tau_x \varphi_x + \tau_y \varphi_y)\right] R(\tau_x, \tau_y)\, d\tau_x\, d\tau_y \tag{A3}$$

Hence, by means of the inverse Fourier transform the correlation function is obtained.

$$R(\tau_x, \tau_y) = \int_{-\infty}^{\infty} \int_{-\infty}^{\infty} \exp\left[i(\tau_x \varphi_x + \tau_y \varphi_y)\right] \mathscr{S}(\varphi_x, \varphi_y)\, d\varphi_x\, d\varphi_y \tag{A4}$$

The correlation function is a characterization of the surface in the x-y plane; the psd is a characterization of the surface in the frequency domain, where φ_x and φ_y

are frequencies. That is, a random surface $z(x, y)$ may be thought of as a superposition of many surface waves of different wavelength, as follows:

$$z(x, y) = \lim_{N \to \infty} \sigma \left(\frac{2}{N}\right)^{1/2} \sum_{n=1}^{N} \cos \left(x\varphi_{x,n} + y\varphi_{y,n} + \epsilon_n\right)$$

where the frequency pairs $(\varphi_{x,n}, \varphi_{y,n})$ are independent random observations from a bivariate probability distribution with joint probability density function $\mathcal{S}(\varphi_x, \varphi_y)$. The ϵ_n are phase factors that are independent random observations from a uniform distribution over $[0, 2\pi]$. Frequencies at which the psd is largest contribute more cosine terms; frequencies at which it is smallest contribute the least. Shinozuka (ref. 25) expands on this representation and uses this technique to simulate multidimensional processes.

Spectral Moments

The interpretation of the psd as a probability density function leads naturally to considering the moments of that distribution as descriptors of its shape. In fact, several authors (refs. 13 to 17) have shown that many geometrical properties (such as peak heights, curvature, and crossings) are determined by functions of the lower order spectral moments. These moments, m_{ij}, are defined here as

$$m_{ij} = \sigma^2 \int_{-\infty}^{\infty} \int_{-\infty}^{\infty} \varphi_x^i \varphi_y^j \mathcal{S}(\varphi_x, \varphi_y)\, d\varphi_x\, d\varphi_y \tag{A5}$$

The psd $\mathcal{S}(x, y)$, as defined here, is truly a probability density function. Thus, strictly speaking, the m_{ij} as defined by equation (A5) should not include the factor σ^2. The reason for including it in this way is so the spectral moments defined herein will correspond to the definition of spectral moments as presented by Longuet-Higgins and Nayak (refs. 13 to 17).

From equation (A5), $m_{00} = \sigma^2$, which is the variance of $z(x, y)$. The quantities m_{20}/σ^2, m_{02}/σ^2, and m_{11}/σ^2 represent the variances and covariances of the frequency distribution, respectively. That is, m_{20}/σ^2 is a descriptor of the spread of the marginal distribution of φ_x, and m_{02}/σ^2 is a descriptor of the spread of the marginal distribution of φ_y, while m_{11}/σ^2 describes the covariance of φ_x and φ_y.

Single Profile Analysis

Webber (ref. 24) and Williamson and Hunt (ref. 26) have discussed methods of estimating the psd of the surface from measurements taken on a grid of points in the x-y plane or from a series of parallel traces. From the spectrum estimate, the spectral moments may be calculated. Nayak (ref. 13), however, has discussed a method of estimating the two-dimensional moments from a series of one-dimensional profiles obtained in several different directions. This method is explained here.

Relation between surface and profile power spectral densities. - Consider a straight line through the origin in the x-y plane and at an angle θ to the x-axis. The height of the surface above this line is a one-dimensional random function of r, the distance from the origin. The correlation function and psd are defined by

$$R_\theta(\tau) = \frac{1}{\sigma^2} E\{[Z(r) - \mu][Z(r + \tau) - \mu]\} \tag{A6}$$

and

$$\mathcal{S}_\theta(\varphi) = \frac{1}{2\pi} \int_{-\infty}^{\infty} R_\theta(\tau) e^{-i\varphi\tau} \, d\tau \tag{A7}$$

The moments of the profile spectrum are calculated by

$$m_{n,\theta} = \int_{-\infty}^{\infty} \varphi^n \mathcal{S}_\theta(\varphi) \, d\varphi \tag{A8}$$

The moments of profile psd's and the surface psd are related by the following equation (ref. 13):

$$m_{n,\theta} = \sum_{k=0}^{n} \binom{n}{k} m_{n-k,k} \sin^k\theta \cos^{n-k}\theta \tag{A9}$$

where $\binom{n}{k}$ denotes the number of combinations of n things taken k at a time.

Isotropic random surfaces. - For isotropic random surfaces the surface profile psd's are the same in every direction. Under isotropic conditions the correlation function $R(\tau_x, \tau_y)$ can be written as $R(r)$, where $r^2 = \tau_x^2 + \tau_y^2$; and the psd $\mathcal{S}(\varphi_x, \varphi_h)$ can be written as $\mathcal{S}(\varphi^*)$, where $(\varphi^*)^2 = \varphi_x^2 + \varphi_y^2$. Therefore, the spectral moments are related as follows:

$$\left.\begin{aligned} m_{11} = m_{13} = m_{31} = 0 \\ m_{20} = m_{02} = m_2 \\ m_{40} = m_{04} = 3m_{22} = m_4 \end{aligned}\right\} \qquad \text{(A10)}$$

APPENDIX B

SUMMITS AND LEVEL CROSSINGS

Surface characterizations relevant to this study are the number of summits per unit area, the probability distribution of the summit heights, and the number of excursions of the surface above a reference level per unit area.

The first two characterizations have been extensively dealt with by Longuet-Higgins (refs. 14 to 16) and Nayak (ref. 13). The third has been considered in an approximate manner by Sidik (ref. 19) and in a more direct but also approximate manner by Adler and Hasofer (ref. 20).

To calculate the distribution of summit heights, first assume $z(x, y)$ to be an ergodic Gaussian random surface process and let the following variables ξ_i $(i = 1, 6)$ be defined:

$$\left.\begin{aligned}
\xi_1 = \xi_1(x, y) &\equiv \frac{\partial^2}{\partial x^2} z(x, y) \\
\xi_2 = \xi_2(x, y) &\equiv \frac{\partial^2}{\partial x \partial y} z(x, y) \\
\xi_3 = \xi_3(x, y) &\equiv \frac{\partial^2}{\partial y^2} z(x, y) \\
\xi_4 = \xi_4(x, y) &\equiv z(x, y) \\
\xi_5 = \xi_5(x, y) &\equiv \frac{\partial}{\partial x} z(x, y) \\
\xi_6 = \xi_6(x, y) &\equiv \frac{\partial}{\partial y} z(x, y)
\end{aligned}\right\} \tag{B1}$$

It is well known (ref. 13) that $\xi^T = (\xi_1, \ldots, \xi_6)$ follows a multivariate normal distribution. The expected number of summits of height ξ_4 within a unit area is given by the triple integral

$$f(\xi_4) = \frac{1}{|\mathscr{F}|^{1/2}|S|^{1/2}(2\pi)^3} \iiint_V |\xi_1\xi_3 - \xi_2^2| e^{-(1/2)Q}\, d\xi_1\, d\xi_2\, d\xi_3 \tag{B2}$$

where the region of integration V is defined by

$$\left.\begin{aligned} \xi_1 &\le 0 \\ \xi_3 &\le 0 \\ \xi_1\xi_3 - \xi_2^2 &\ge 0 \end{aligned}\right\} \tag{B3}$$

and

$$\mathscr{F} = \begin{bmatrix} m_{40} & m_{31} & m_{22} & -m_{20} \\ m_{31} & m_{22} & m_{13} & -m_{11} \\ m_{22} & m_{13} & m_{04} & -m_{02} \\ -m_{20} & -m_{11} & -m_{02} & m_{00} \end{bmatrix} \tag{B4}$$

$$S = \begin{bmatrix} m_{20} & m_{11} \\ m_{11} & m_{02} \end{bmatrix} \tag{B5}$$

$$Q = (\xi_1, \xi_2, \xi_3, \xi_4)\mathscr{F}^{-1}(\xi_1, \xi_2, \xi_3, \xi_4)^T \tag{B6}$$

Equation (B2) was transformed to cylindrical coordinates followed by a rotation. The transformation equations are

$$\left.\begin{aligned} \xi_1 &= \frac{r - \rho\cos\varphi}{\sqrt{2}} \\ \xi_2 &= \frac{\rho\sin\varphi}{\sqrt{2}} \\ \xi_3 &= \frac{r + \rho\cos\varphi}{\sqrt{2}} \\ \xi_4 &= \Lambda m_{00}^{1/2} \end{aligned}\right\} \tag{B7}$$

It now becomes evident that the region V describes a semi-infinite cone, as shown by the limits of integration on the transformed equation.

$$f(\Lambda) = \frac{1}{|\mathcal{F}|^{1/2}|S|^{1/2}(2\pi)^3}\int_{r=0}^{\infty}\int_{\rho=0}^{r}\int_{\varphi=0}^{2\pi}\frac{(r^2 - \rho^2)\rho}{2^{3/2}}\, e^{-(1/2)Q}\, d\varphi\, d\rho\, dr \tag{B8}$$

$$Q = \begin{bmatrix} \frac{r - \rho\cos\varphi}{\sqrt{2}} \\ \frac{\rho\sin\varphi}{\sqrt{2}} \\ \frac{r + \rho\cos\varphi}{\sqrt{2}} \\ \Lambda \end{bmatrix}^T \begin{bmatrix} m_{40} & m_{31} & m_{22} & \frac{-m_{20}}{m_{00}^{1/2}} \\ m_{31} & m_{22} & m_{13} & \frac{-m_{11}}{m_{00}^{1/2}} \\ m_{22} & m_{13} & m_{04} & \frac{-m_{02}}{m_{00}^{1/2}} \\ \frac{-m_{20}}{m_{00}^{1/2}} & \frac{-m_{11}}{m_{00}^{1/2}} & \frac{-m_{02}}{m_{00}^{1/2}} & 1 \end{bmatrix} \begin{bmatrix} \frac{r - \rho\cos\varphi}{\sqrt{2}} \\ \frac{\rho\sin\varphi}{\sqrt{2}} \\ \frac{r + \rho\cos\varphi}{\sqrt{2}} \\ \Lambda \end{bmatrix} \tag{B9}$$

Equation (B8) was evaluated numerically on the digital computer. The expected number of summits per unit area D_{sum} is given by the integral

$$D_{sum} = \int_{-\infty}^{\infty} f(\Lambda)\, d\Lambda \tag{B10}$$

The probability density for summit heights is given by the ratio

$$p^*(\Lambda) = \frac{f(\Lambda)}{D_{sum}} \tag{B11}$$

The expected number of excursions above level Λ per unit area is approximated by the product of peaks per unit area and the proportion of such peaks that exceed the level Λ.

$$E\{\chi(\Lambda)\} \approx D_{sum} \int_{\xi=\Lambda}^{\infty} p^*(\xi)\, d\xi = \int_{\xi=\Lambda}^{\infty} f(\xi)\, d\xi \tag{B12}$$

This approximation is valid only in the limiting sense as $\Lambda \to \infty$.

Adler and Hasofer (ref. 20) also provide an approximation for the upcrossings of a process $z(x, y)$ over the level Λ. In terms of the present notation, their results are given by the relation

$$E\{\chi(\Lambda)\} \approx \frac{\Lambda |S|^{1/2} \exp\left(-\frac{\Lambda^2}{2}\right)}{(2\pi)^{3/2}\, \sigma^2} \tag{B13}$$

It is interesting to note that this expression does not involve any fourth-order moments.

REFERENCES

1. Hertz, Heinrich (B. E. Jones and G. A. Schott, transl.): Part V - The Contact of Elastic Solids. Miscellaneous Papers, Macmillan Co., 1896, pp. 146-162.

2. Dowson, D.; and Higginson, G. R.: Elastohydrodynamic Lubrication. Pergamon Press, 1966.

3. Zaretsky, E. V.; and Anderson, W. J.: EHD Lubrication. Mach. Des., vol. 40, Nov. 7, 1968, pp. 167-173.

4. Tallian, T. E.: Elastohydrodynamic Hertzian Contacts - Part 1. Mech. Eng., vol. 93, no. 11, Nov. 1971, pp. 14-18.

5. Tallian, T. E.: Elastohydrodynamic Hertzian Contacts - Part 2. Mech. Eng., vol. 93, no. 12, Dec. 1971, pp. 17-22.

6. Bamberger, E. N., et al.: Life Adjustment Factors for Ball and Roller Bearings - An Engineering Design Guide. American Soc. Mech. Eng., 1971.

7. Seth, B. B.; and Willis, T.: Techniques for Film Thickness Measurements in Elastohydrodynamic Lubrication. ASME paper 76-DET-79, Sept. 1976.

8. Tallian, T. E.; et al.: Lubricant Films in Rolling Contact of Rough Surfaces. Trans. ASLE, vol. 7, no. 2, Apr. 1964, pp. 109-126.

9. Tallian, T. E.: The Theory of Partial Elastohydrodynamic Contacts. Wear, 21, 1972, pp. 49-101.

10. Whitehouse, D. J.; and Archard, J. F.: The Properties of Random Surfaces of Significance in their Contact. Proc. R. Soc. London, Ser. A, vol. 316, no. 1524, Mar. 1970, pp. 97-121.

11. Johnson, K. L.; Greenwood, J. A.; and Poon, S. Y.: A Simple Theory of Asperity Contact in Elastohydrodynamic Lubrication. Wear, vol. 19, 1972, pp. 91-108.

12. Archard, J. F.: Surface Topography and Tribology. Tribol. Int., vol. 7, no. 5, Oct. 1974, pp. 213-220.

13. Nayak, P. Ranganath: Random Process Model of Rough Surfaces. J. Lubr. Technol., vol. 93, no. 3, July 1971, pp. 398-407.

14. Longuet-Higgins, M. S.: The Statistical Analysis of a Random, Moving Surface. Philos. Trans. R. Soc. London, Ser. A, vol. 249, no. 966, 1956-1957, pp. 321-387.

15. Longuet-Higgins, M. S.: Statistical Properties of an Isotropic Random Surface. Philos. Trans. R. Soc. London, Ser. A, vol. 250, no. 975, 1957-1958, pp. 157-174.

16. Longuet-Higgins, M. S.: The Statistical Geometry of Random Surfaces. Hydrodynamic Instability, Proceedings of the 13th Symposium on Applied Mathematics, Amer. Math. Soc., 1962, pp. 105-143.

17. Nayak, P. Ranganath: Some Aspects of Surface Roughness Measurement. Wear, vol. 26, 1973, pp. 165-174.

18. Sidik, Steven M.: Analysis of Electrical Contact Occurrences Between Rolling Surfaces with Application to Elastohydrodynamic Lubrication. NASA TN D-7134, 1973.

19. Sidik, Steven M.: Two-Dimensional Gaussian Processes Applied to the Determination of Contact Between Lubricated Rolling Surfaces. NASA TM X-71598, 1974.

20. Adler, Robert J.; and Hasofer, A. M.: Level Crossings for Random Fields. Annals of Probability, vol. 4, no. 1, Feb. 1976, pp. 1-12.

21. Lindgren, Georg: Spectral Moment Estimation by Means of Level Crossings. Biometrika, vol. 61, no. 3, 1974, pp. 401-418.

22. Cramer, Harald; and Leadbetter, M. R.: Stationary and Related Stochastic Processes. John Wiley & Sons, Inc., 1967.

23. Collatz, Lothar: The Numerical Treatment of Differential Equations. Third ed. Springer-Verlag, 1966.

24. Webber, William Fred: On the Statistical Analysis of Random Surfaces. Ph.D. Thesis, Southern Methodist Univ., 1971.

25. Shinozuka, M.: Simulation of Multivariate and Multidimensional Random Processes. J. Acoust. Soc. Am., vol. 49, no. 1 (pt. 2), 1971, pp. 357-368.

26. Williamson, J. B. P.; and Hunt, R. T.: Relocation Profilometry. J. Phys. E., Ser. 2, vol. 1, July 1968, pp. 749-752.

TABLE I. - HERTZIAN CONTACT CONDITIONS AT INNER AND OUTER RACES FOR THREE THRUST LOADS

[Width of rolling track is determined by major axis width.]

Race	Contact condition	Thrust load, N (lbf)		
		90 (20)	445 (100)	3100 (700)
Inner	Maximum Hertzian stress, GPa (ksi)	1.28 (185)	2.09 (303)	3.63 (527)
	Semimajor axis, cm (in.)	0.0510 (0.0200)	0.0840 (0.0330)	0.1500 (0.0570)
	Semiminor axis, cm (in.)	0.0066 (0.0026)	0.0110 (0.0043)	0.0190 (0.0076)
Outer	Maximum Hertzian stress, GPa (ksi)	1.13 (164)	1.85 (269)	3.27 (474)
	Semimajor axis, cm (in.)	0.0460 (0.0180)	0.0740 (0.0290)	0.1300 (0.0500)
	Semiminor axis, cm (in.)	0.0086 (0.0034)	0.0140 (0.0055)	0.0250 (0.0097)

TABLE II. - DIGITIZATION SAMPLE INTERVALS, NUMBER OF SAMPLE POINTS, AND TOTAL LENGTH OF SURFACE PROFILE SAMPLED

Trace	Profile	Sample interval, Δ, μm	Sample points, N	Sampled length, cm
1	Ball, 0°	0.94	14 220	1.30
2	Ball, 45°	.75	32 232	2.40
3	Ball, 90°	.71	9 954	.70
4	Flat, 0°	0.31	29 388	0.90
5	Flat, 18°		25 122	.77
6	Flat, 36°		27 492	.84
7	Flat, 54°		29 388	.90
8	Flat, 72°		29 388	.90
9	Flat, 90°		25 122	.77
10	Flat, 90° (repeat)		28 440	.87

TABLE III. - TOTAL NUMBER OF SAMPLE POINTS

USED IN COMPUTING MOVING AVERAGE

Trace	Profile	Thrust load, N (lb)		
		90 (20)	445 (100)	3100 (700)
1	Ball, 0^{o}	2163	3 567	6 163
2	Ball, 45^{o}	2711	4 475	7 729
3	Ball, 90^{o}	2857	4 715	8 143
4	Flat, 0^{o}	6623	10 927	18 875
5	Flat, 18^{o}	↓	↓	↓
6	Flat, 36^{o}			
7	Flat, 54^{o}			
8	Flat, 72^{o}			
9	Flat, 90^{o}			
10	Flat, 90^{o} (repeat)			

TABLE IV. - ESTIMATES OF SPECTRA L MOMENTS

Trace	Profile	Thrust load, N (lb)								
		90 (20)	445 (100)	3100 (700)	90 (20)	445 (100)	3100 (700)	90 (20)	445 (100)	3100 (700)
		Profile spectral moments								
		m_0, μm^2			m_2, dimensionless			m_4, μm^{-2}		
1	Ball, 0^{o}	1.90×10^{-3}	1.92×10^{-3}	1.91×10^{-3}	8.48×10^{-5}	8.49×10^{-5}	7.56×10^{-5}	4.07×10^{-5}	4.21×10^{-5}	3.04×10^{-5}
2	Ball, 45^{o}	1.86×10^{-3}	2.01×10^{-3}	2.27×10^{-3}	1.66×10^{-4}	1.67×10^{-4}	1.68×10^{-4}	1.22×10^{-4}	1.23×10^{-4}	1.24×10^{-4}
3	Ball, 90^{o}	1.81×10^{-3}	1.69×10^{-3}	1.29×10^{-3}	1.66×10^{-4}	1.63×10^{-4}	1.38×10^{-4}	1.13×10^{-4}	1.12×10^{-4}	1.01×10^{-4}
4	Flat, 0^{o}	7.94×10^{-2}	9.84×10^{-2}	6.12×10^{-2}	2.12×10^{-3}	2.11×10^{-3}	2.06×10^{-3}	6.64×10^{-2}	6.61×10^{-2}	6.49×10^{-2}
5	Flat, 18^{o}	6.59×10^{-2}	6.99×10^{-2}	4.22×10^{-2}	2.65×10^{-3}	2.69×10^{-3}	2.57×10^{-3}	6.55×10^{-2}	6.67×10^{-2}	6.71×10^{-2}
6	Flat, 36^{o}	5.55×10^{-2}	6.19×10^{-2}	6.91×10^{-2}	3.62×10^{-3}	3.64×10^{-3}	3.40×10^{-3}	6.44×10^{-2}	6.47×10^{-2}	6.56×10^{-2}
7	Flat, 54^{o}	6.06×10^{-2}	6.37×10^{-2}	7.58×10^{-2}	4.38×10^{-3}	4.46×10^{-3}	4.42×10^{-3}	6.77×10^{-2}	6.74×10^{-2}	6.83×10^{-2}
8	Flat, 72^{o}	4.45×10^{-2}	4.42×10^{-2}	4.97×10^{-2}	5.07×10^{-3}	5.19×10^{-3}	5.08×10^{-3}	7.20×10^{-2}	7.25×10^{-2}	7.21×10^{-2}
9	Flat, 90^{o}	4.99×10^{-2}	4.73×10^{-2}	5.18×10^{-2}	5.65×10^{-3}	5.62×10^{-3}	5.82×10^{-3}	7.14×10^{-2}	7.12×10^{-2}	6.89×10^{-2}
10	Flat, 90^{o} (repeat)	4.96×10^{-2}	4.98×10^{-2}	5.05×10^{-2}	5.72×10^{-3}	5.68×10^{-3}	5.66×10^{-3}	7.39×10^{-2}	7.29×10^{-2}	7.21×10^{-2}

TABLE V. - CORRELATION FUNCTION ESTIMATES AND SPECTRAL MOMENTS GENERATED BY USING EQUATION (12)

[Load, 90 N (20 lbf).]

Trace	Profile	Correlation					Spectral moment calculated by equation (12)		
		R_1	R_2	R_3	R_4	R_5	m_0, μm^2	m_2	m_4, μm^{-2}
1	Ball, 0°	0.9802	0.9293	0.8623	0.7903	0.7198	1.90×10^{-3}	8.52×10^{-5}	4.17×10^{-5}
2	Ball, 45°	.9750	.9103	.8258	.7387	.6603	1.86×10^{-3}	1.66×10^{-4}	1.24×10^{-4}
3	Ball, 90°	.9750	.9119	.8263	.7327	.6433	1.81×10^{-3}	1.80×10^{-4}	1.70×10^{-4}
4	Flat, 0°	0.9987	0.9987	0.9984	0.9981	0.9978	7.94×10^{-2}	2.12×10^{-2}	6.64×10^{-2}
5	Flat, 18°	.9981	.9968	.9946	.9917	.9881	6.59×10^{-2}	2.67×10^{-2}	6.60×10^{-2}
6	Flat, 36°	.9969	.9927	.9859	.9769	.9660	5.55×10^{-2}	3.71×10^{-2}	6.62×10^{-2}
7	Flat, 54°	.9966	.9913	.9826	.9714	.9580	6.06×10^{-2}	4.42×10^{-2}	6.85×10^{-2}
8	Flat, 72°	.9946	.9857	.9712	.9526	.9308	4.45×10^{-2}	5.10×10^{-2}	7.25×10^{-2}
9	Flat, 90°	.9942	.9840	.9681	.9480	.9247	4.99×10^{-2}	6.15×10^{-2}	8.13×10^{-2}
10	Flat, 90° (repeat)	.9945	.9847	.9690	.9491	.9261	4.96×10^{-2}	5.83×10^{-2}	7.61×10^{-2}

TABLE VI. - DIMENSIONLESS CONTACT FRACTIONS GENERATED BY USING EQUATION (B12)

Load		Dimensionless film thickness,	Summits of height Λ per square centimeter,	Excursions above level Λ per square centimeter,	Dimensionless contact fractions		
N	lbf	Λ	$f(\Lambda)$	$E(\chi)$	$T_{c,in}$	$T_{c,out}$	$T_{c,ov}$
90	20	4.35	3018	679.8	0.717	0.843	0.938
90	20	4.40	2440	543.9	.573	.675	.770
90	20	4.50	1584	345.7	.364	.429	.399
90	20	4.60	1017	217.5	.229	.270	.174
90	20	4.70	647	135.6	.143	.168	.0704
90	20	4.80	407	83.7	.088	.104	.0273
90	20	4.90	254	51.2	.054	.064	.0103
90	20	5.00	157	31.1	.033	.039	.00378
90	20	5.10	96	18.7	.020	.023	.00137
445	100	4.55	1242	267.8	0.771	0.866	0.963
445	100	4.60	994	212.2	.610	.686	.804
445	100	4.70	632	132.2	.380	.428	.413
445	100	4.80	398	81.6	.235	.264	.175
445	100	4.90	248	49.9	.144	.161	.0679
445	100	5.00	153	30.3	.087	.098	.0253
445	100	5.10	93	18.2	.052	.059	.00918
3100	700	4.80	403	82.8	0.727	0.814	0.932
3100	700	4.90	251	50.6	.444	.498	.528
3100	700	5.00	155	30.7	.269	.302	.224
3100	700	5.10	95	18.4	.162	.181	.0851
3100	700	5.20	57	10.9	.096	.108	.0307
3100	700	5.30	34	6.4	.057	.063	.0107

TABLE VII. - DIMENSIONLESS CONTACT FRACTIONS GENERATED BY USING EQUATION (B13)

Load		Dimensionless film thickness,	Expected number of excursions above level Λ per square centimeter,	Dimensionless contact fraction		
N	lbf	Λ	$E(\chi)$	$T_{c,in}$	$T_{c,out}$	$T_{c,ov}$
90	20	3.90	763.1	0.804	0.947	0.986
90	20	4.0	527.3	.556	.654	.742
90	20	4.1	360.5	.380	.447	.428
90	20	4.2	243.8	.257	.303	.216
90	20	4.3	163.2	.172	.202	.101
90	20	4.4	108.1	.114	.134	.0452
90	20	4.5	70.9	.075	.088	.0196
90	20	4.6	45.9	.048	.057	.00826
90	20	4.7	29.6	.031	.037	.00341
90	20	4.8	18.7	.020	.023	.00138
90	20	4.9	11.8	.012	.015	.000544
445	100	4.2	216.4	0.622	0.700	0.820
445	100	4.3	144.8	.417	.468	.478
445	100	4.4	95.9	.276	.310	.235
445	100	4.5	62.9	.181	.203	.106
445	100	4.6	40.8	.117	.132	.0457
445	100	4.7	26.2	.075	.085	.0190
445	100	4.8	16.6	.048	.054	.00769
445	100	4.9	10.4	.030	.034	.00304
445	100	5.0	6.5	.019	.021	.00118
445	100	5.1	4.0	.012	.013	.000446
3100	700	4.5	68.0	0.597	0.668	0.783
3100	700	4.6	44.1	.387	.443	.424
3100	700	4.7	28.3	.248	.278	.193
3100	700	4.8	18.0	.158	.177	.0813
3100	700	4.9	11.3	.099	.111	.0327
3100	700	5.0	7.0	.062	.069	.0127
3100	700	5.1	4.3	.038	.043	.00483
3100	700	5.2	2.6	.023	.026	.00180
3100	700	5.3	1.6	.014	.016	.000653

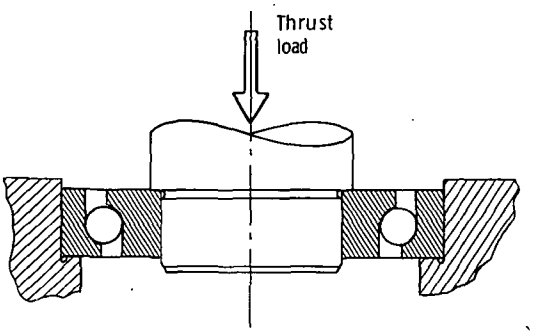

Figure 1. - Typical thrust-loaded ball bearing.

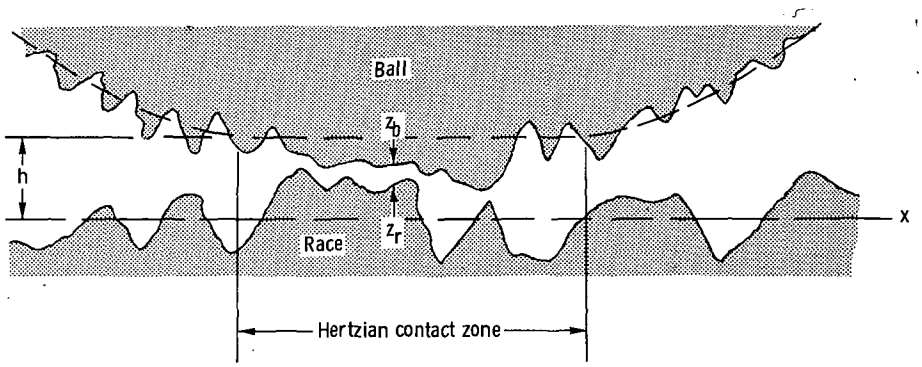

Figure 2. - Cross section of ball-race contact. (Surface roughness is greatly exaggerated.)

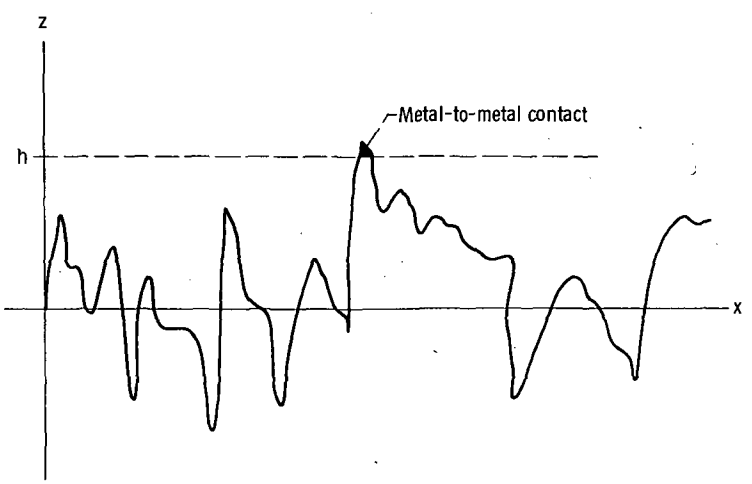

Figure 3. - Cross section of a composite surface roughness process.

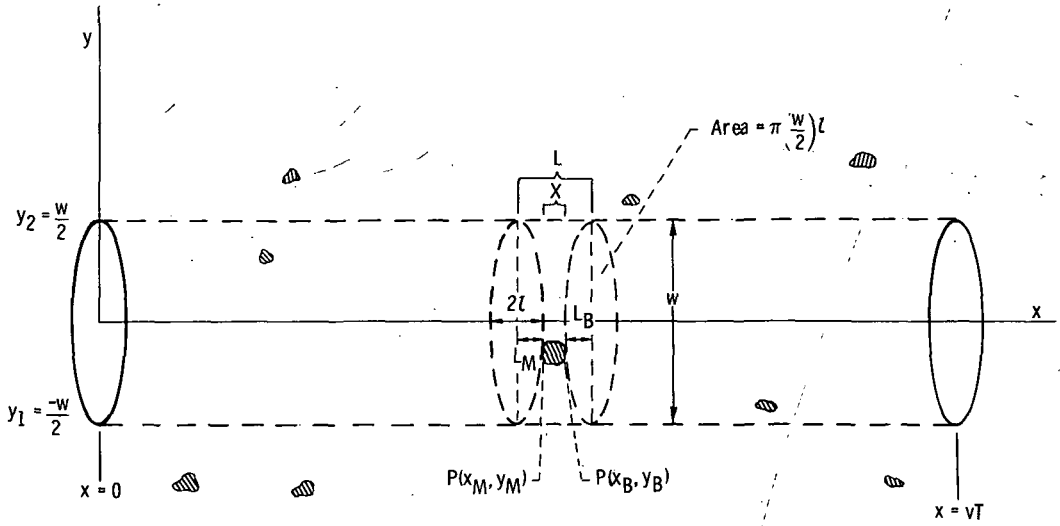

Figure 4. - Typical contact occurrence when contact areas are small.

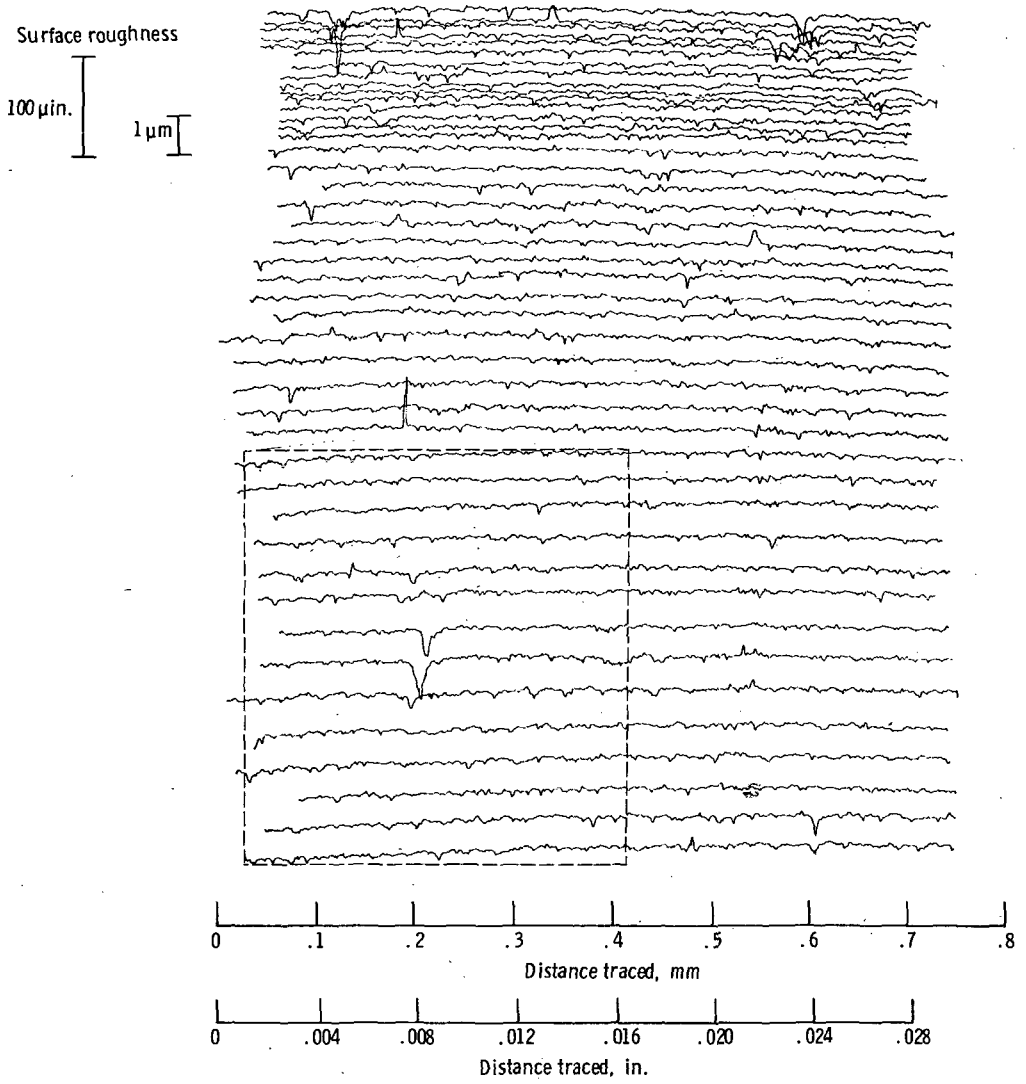

(a) Nominal trace spacing, 13 micrometers (0.0005 in.); vertical magnification, approximately 40 times horizontal scale. (See fig. 5(b) for enlargement of area within dashed box.)

Figure 5. - Microtopography of ball specimen. Nominal centerline average (CLA) roughness, 0.03 to 0.05 micrometer (1 to 2 μin.).

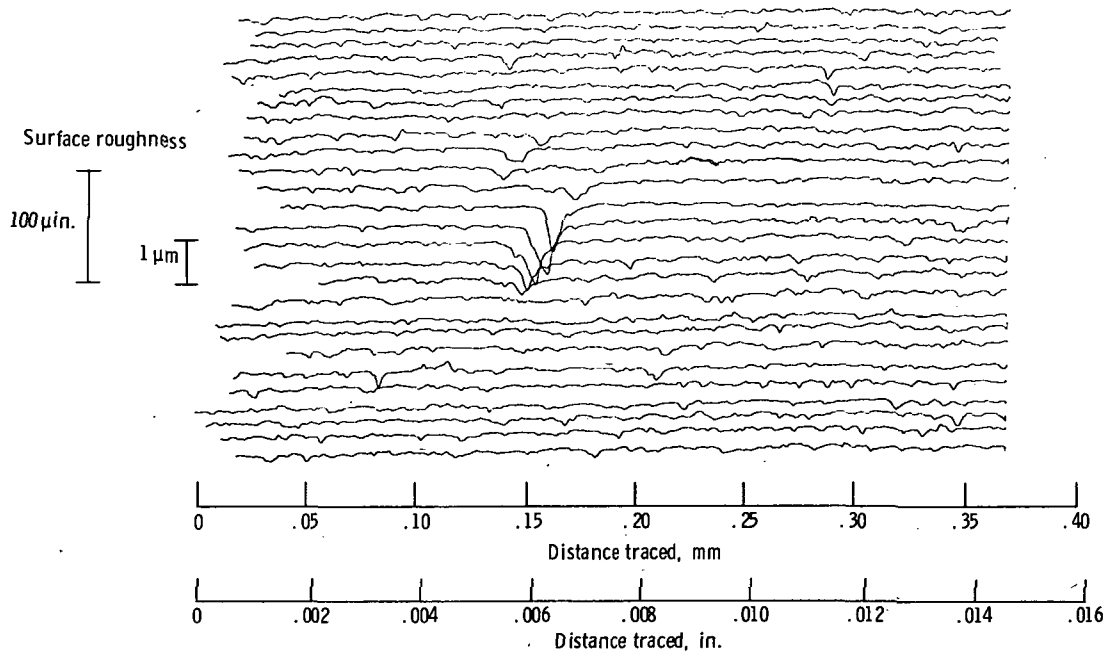

(b) Enlarged view of ball specimen: nominal trace spacing, 6 micrometers (0.00025 in.); vertical magnification, approximately 20 times horizontal scale. (Small surface scratches in random directions are evident.)

Figure 5. - Concluded.

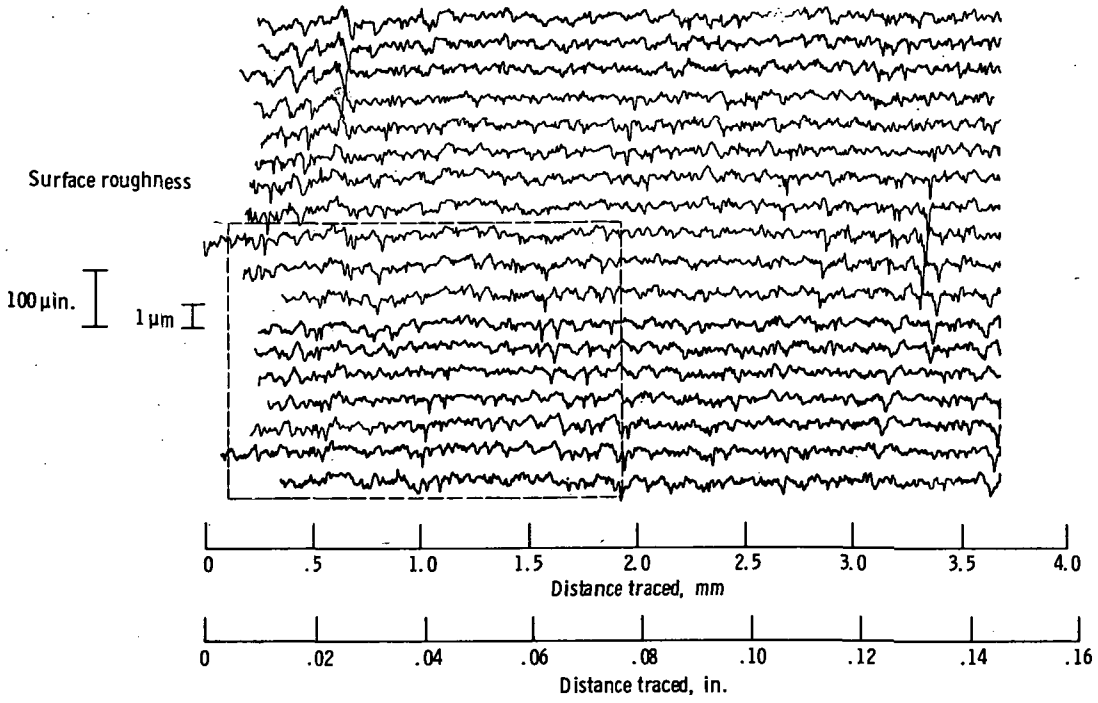

(a) Nominal trace spacing, 130 micrometers (0.005 in.); vertical magnification, approximately 100 times horizontal scale; tracing direction, across lay of surface finish. (See fig. 6(b) for enlargement of area within dashed box.)

Figure 6. - Microtopography of flat specimen. Nominal centerline average (CLA) roughness, 0.13 to 0.25 micrometer (5 to 10 μin.).

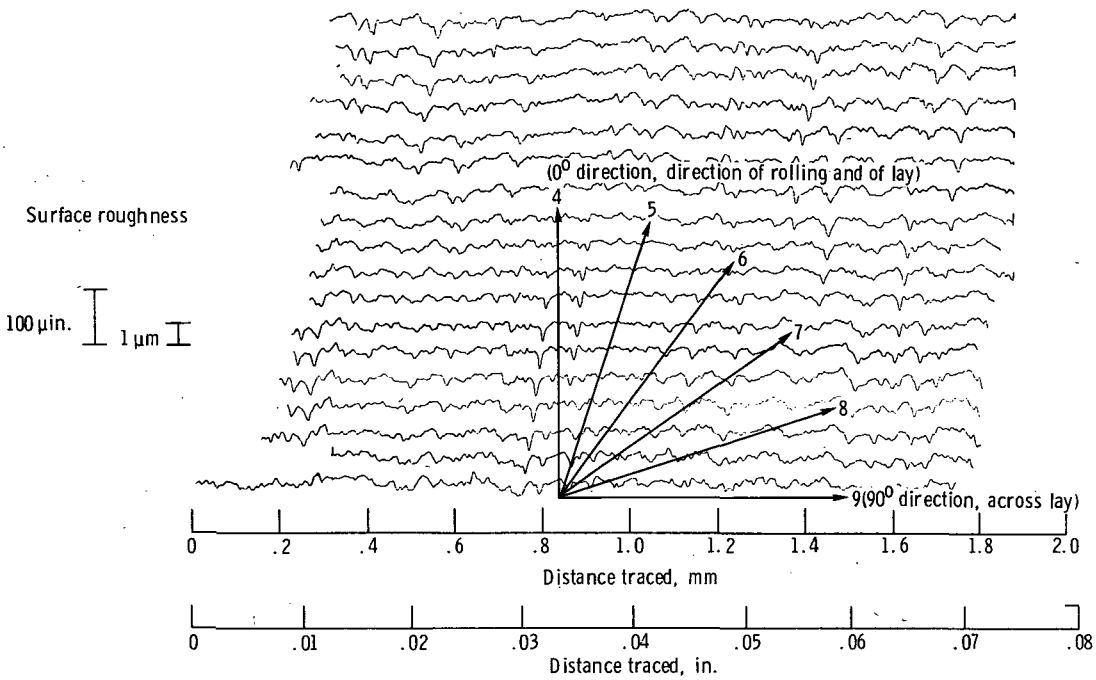

(b) Enlarged view of flat specimen: nominal trace spacing, 64 micrometers (0.0025 in.); vertical magnitifaction, 50 times horizontal scale; tracing directions, denoted by arrows and numbers. (Unidirectional scratches showing lay of surface are clearly evident.)

Figure 6. - Concluded.

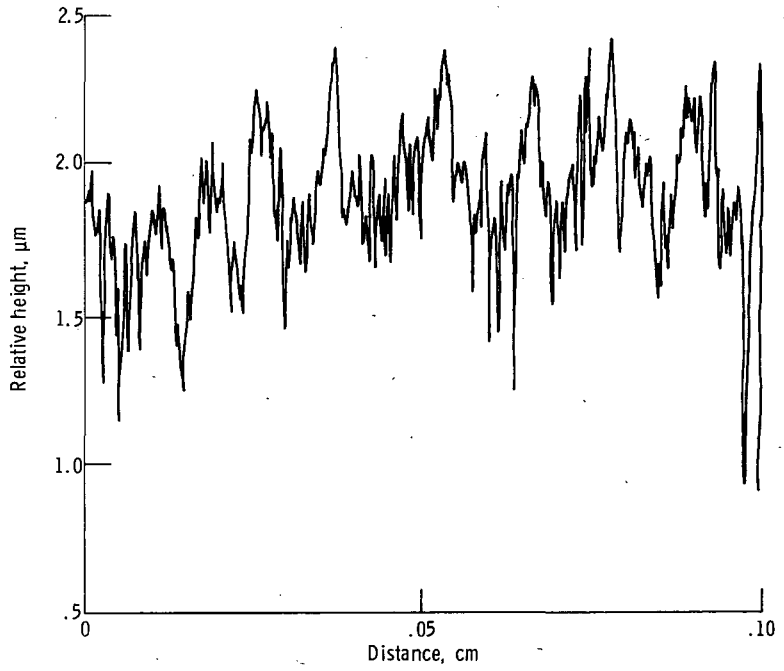

Figure 7. - Raw data plot for profile trace 10. (Flat specimen, 90° (repeat).)

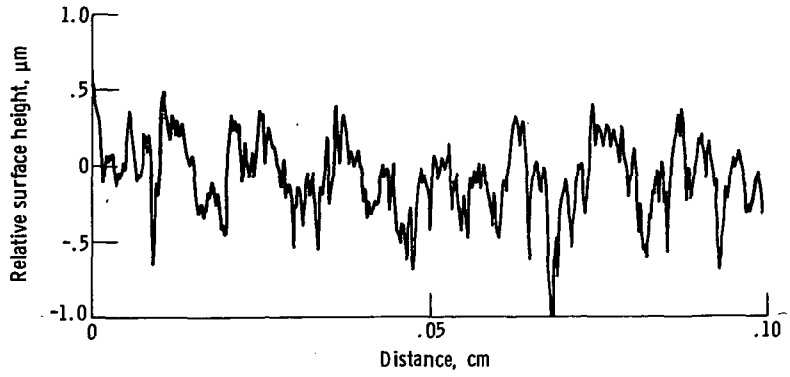

Figure 8. - Centered and detrended data for profile trace 10. Load, 90 newtons (20 lbf).

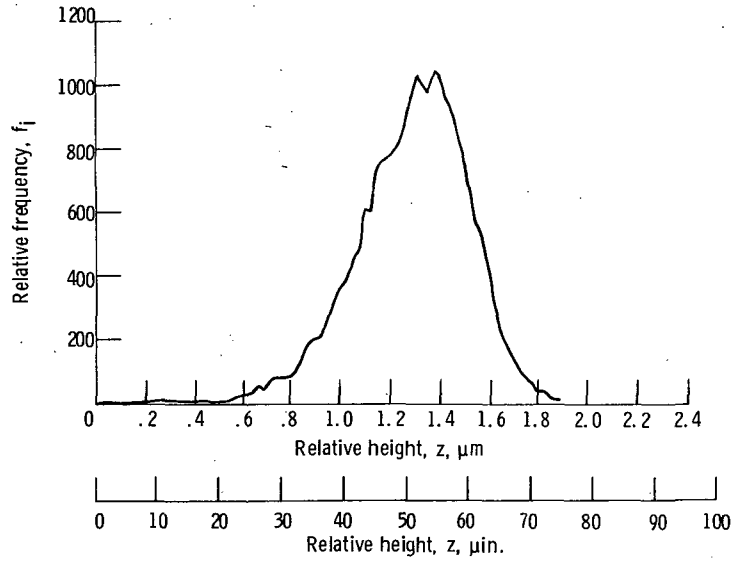

Figure 9. - Frequency polygon for digitized data from profile trace 10. Detrended for 6623 sample points.

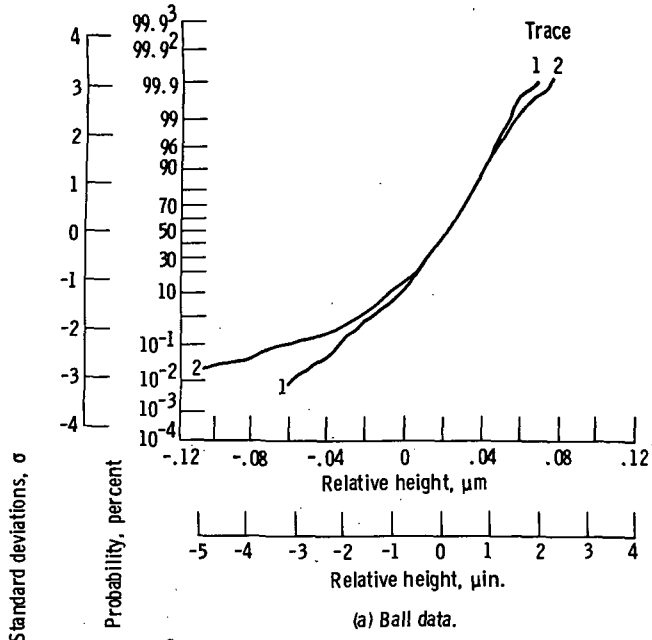

(a) Ball data.

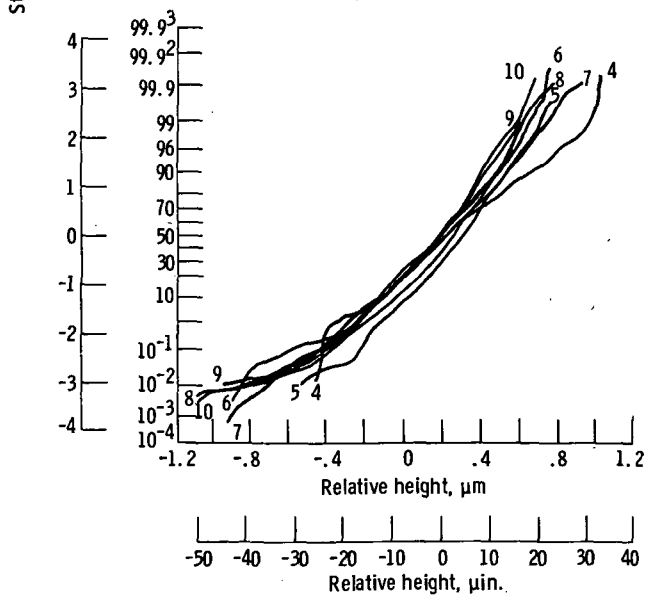

(b) Flat data.

Figure 10. - Cumulative distribution of relative surface height as determined from profile traces in various directions.

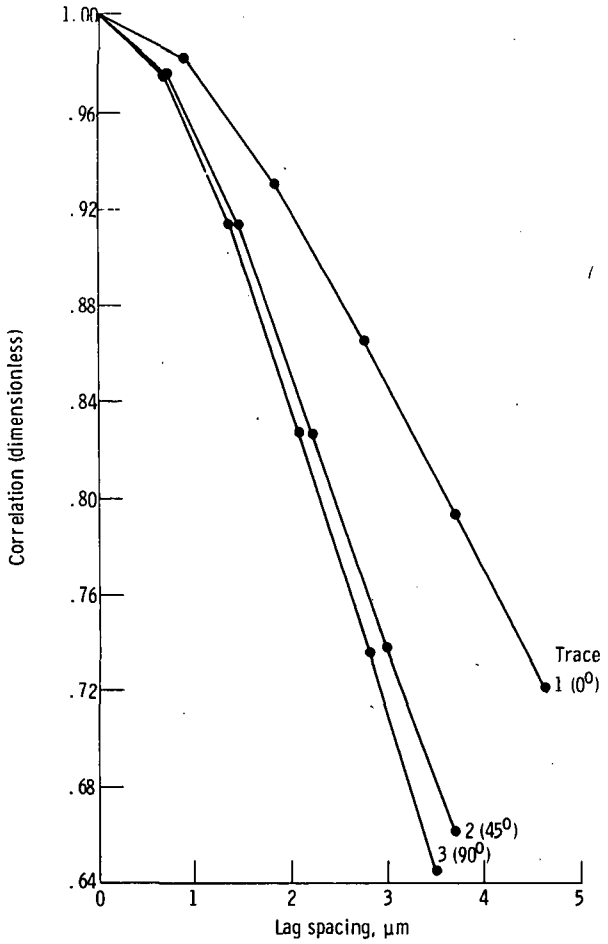

Figure 11. - Correlation function for as many as five lag spacings of ball surface profile traces. Load, 90 newtons (20 lbf).

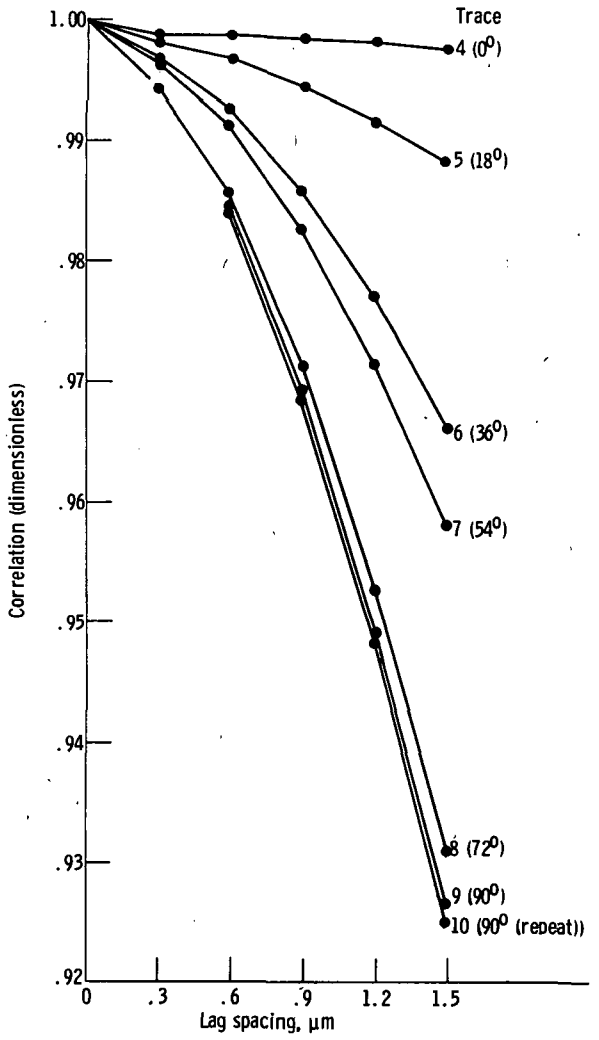

Figure 12. - Correlation function for as many as five lag spacings of flat surface profile traces. Load, 90 newtons (20 lbf).

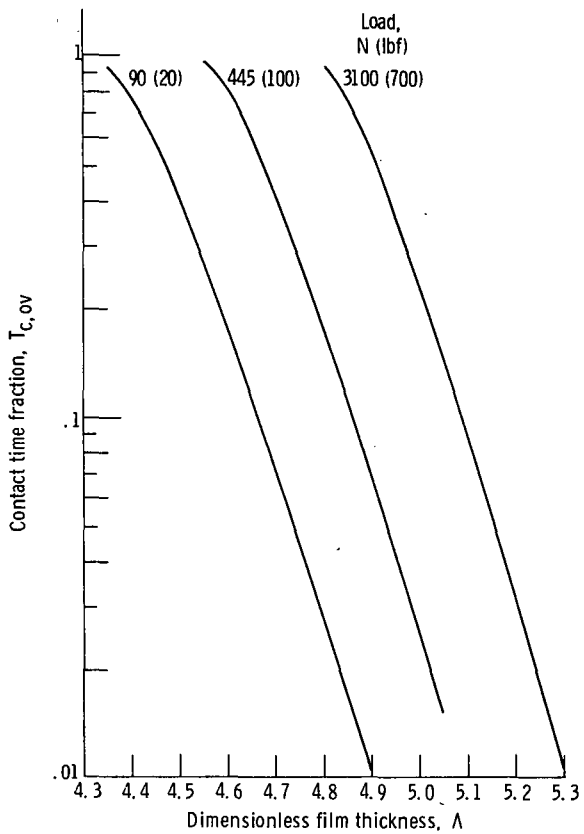

Figure 13. - Overall contact time fraction as function of normalized film thickness for three load conditions - based on present analysis.

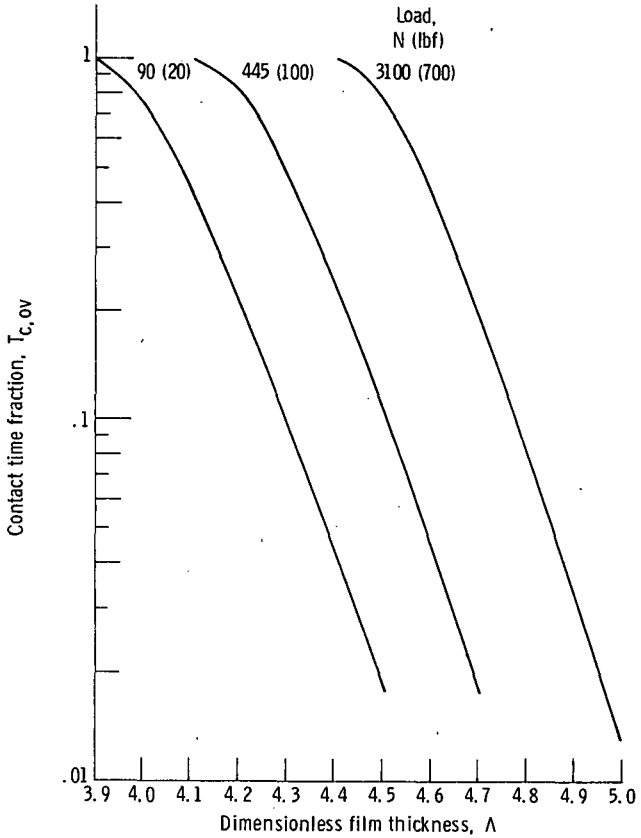

Figure 14. - Overall contact time fraction as function of normalized film thickness - based on method of Adler and Hasofer (ref. 20).

1. Report No.	2. Government Accession No.	3. Recipient's Catalog No.
NASA TP-1130		

4. Title and Subtitle	5. Report Date
STATISTICAL MODEL FOR ASPERITY-CONTACT TIME FRACTION IN ELASTOHYDRODYNAMIC LUBRICATION	February 1978
	6. Performing Organization Code

7. Author(s)	8. Performing Organization Report No.
Steven M. Sidik and John J. Coy	E-9265
	10. Work Unit No. 505-04

9. Performing Organization Name and Address	11. Contract or Grant No.
NASA Lewis Research Center and Propulsion Laboratory U.S. Army R&T Laboratories (AVRADCOM) Cleveland, Ohio 44135	

12. Sponsoring Agency Name and Address	13. Type of Report and Period Covered
National Aeronautics and Space Administration Washington, D.C. 20546	Technical Paper
	14. Sponsoring Agency Code

15. Supplementary Notes

16. Abstract

Relations for the asperity-contact time fraction during elastohydrodynamic (EHD) lubrication of a typical ball bearing are presented. The analysis is based on a two-dimensional random surface model, and actual profile traces of the bearing surfaces were used as statistical sample records. The results of the analysis show that transition from 90-percent contact to 1-percent contact occurs within a dimensionless film thickness range of approximately 4 to 5. This thickness ratio is several times larger than reported in the literature where one-dimensional random surface models were used.

17. Key Words (Suggested by Author(s))	18. Distribution Statement
Lubrication; Friction; Bearings; Statistical geometry; Gaussian random surfaces	Unclassified - unlimited STAR Category 37

19. Security Classif. (of this report)	20. Security Classif. (of this page)	21. No. of Pages	22. Price*
Unclassified	Unclassified	40	A03

* For sale by the National Technical Information Service, Springfield, Virginia 22161

National Aeronautics and Space Administration

Washington, D.C.
20546

Official Business
Penalty for Private Use, $300

THIRD-CLASS BULK RATE

Postage and Fees Paid
National Aeronautics and
Space Administration
NASA-451

NASA

POSTMASTER: If Undeliverable (Section 158 Postal Manual) Do Not Return